Nanoscale

ROYAL SOCIETY OF CHEMISTRY

PAPER

View Article Online
View Journal | View Issue

Cite this: *Nanoscale*, 2024, **16**, 13571

Clustering triggered emissive liquid crystalline template for dual mode upconverted and downconverted circularly polarized luminescence†

Sreelakshmi Theeyanchery Nalavadath, Sonia Maniappan, Anannya Mandal and Jatish Kumar *

Liquid crystalline materials have attracted significant attention in chiroptical research due to their ability to form long range ordered helical superstructures. Research focus has been on exploiting the unique properties of liquid crystalline materials to demonstrate highly dissymmetric circularly polarised luminescent (CPL) systems. In this study, we present a thermally driven, facile approach to fabricate CPL-active materials utilizing cholesteryl benzoate as the active substrate. Cholesteryl benzoate, a well-known thermotropic liquid crystal, has been found to manifest intriguing optical characteristics upon subjecting to repeated heating–cooling cycles. Despite the absence of conventional fluorescent moieties, the material exhibited luminescence through aggregation induced clustering triggered emission mechanism. Systematic investigations revealed excitation-dependent CPL for solid cholesteryl benzoate films when subjected to multiple thermal cycles. The excited state chiroptical investigation performed after multiple thermal cycles showed a luminescence anisotropy (g_{lum}) of 8×10^{-2}, which is a high value for simple organic molecules. Moreover, upon co-assembly with lanthanide-based upconversion nanophosphors (UCNPs), the hybrid system demonstrated upconverted circularly polarised luminescence (UC-CPL). Benefiting from the ability to endow upconversion nanoparticles of various sizes, fabrication of UCNP-ChB hybrid nanocomposites exhibiting multicoloured upconversion CPL was demonstrated. These findings highlight the potential of liquid crystalline materials for diverse applications, including 3D optical displays and anticounterfeiting technologies.

Received 29th February 2024,
Accepted 25th June 2024

DOI: 10.1039/d4nr00865k

rsc.li/nanoscale

Introduction

Circularly polarized luminescence (CPL) is an emergent technique that explores the optical activity of molecules and materials in their excited state. Design and development of innovative materials exhibiting high CPL activity has become an imperative pursuit of researchers due to its endless applications in diverse fields ranging from chemistry, biology and material science.[1–5] CPL activity not only signifies the chiral emissive characteristics of a material but also holds pivotal significance in the analysis of chirality transmission and amplification,[6] thereby offering avenues for advancement in biosensing,[7,8] catalysis,[9] photoelectric devices,[10] and 3D displays.[11] The imperative quest lies in the development of CPL-active materials with high dissymmetry factors and tunable optical properties, prompting extensive investigations into the CPL active materials. Chiral induction at the nanoscale can be achieved through various strategic approaches, namely structural chirality,[12,13] induced chirality,[14,15] and template-assisted chirality.[16] Among the various methods adopted, the template-assisted approach stands out as a promising technique for inducing chirality in achiral luminescent materials, thereby generating chiral emission. Various templates, such as liquid crystalline materials,[17] DNA,[18,19] peptides,[20,21] and organogelators,[22,23] have been actively explored for this purpose. Liquid crystalline materials, owing to their ability to form profound long-range chiral helical superstructures, have been exploited as efficient template for chiral induction. High dissymmetry factor and tunable optical properties are attributes that render thermotropic liquid crystals as front runners in chiral templating of nanoparticles.

Clustering triggered emission (CTE) is a unique phenomenon gaining vast research attention in recent years for developing materials, typically using molecules that lack conventional aromatic luminescent moieties.[24,25] It is of prime sig-

Department of Chemistry, Indian Institute of Science Education and Research (IISER) Tirupati, Tirupati 517507, India. E-mail: jatish@iisertirupati.ac.in

† Electronic supplementary information (ESI) available. See DOI: https://doi.org/10.1039/d4nr00865k

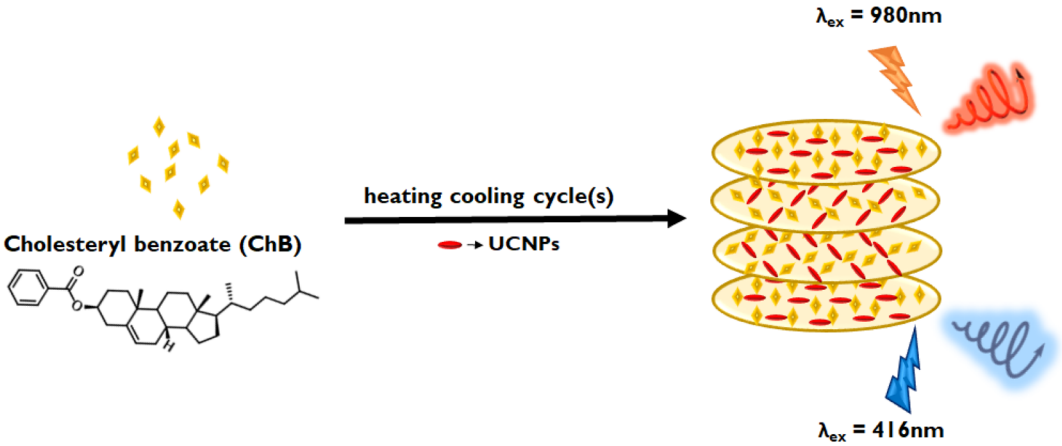

Fig. 1 Scheme depicting the generation of upconverted (top) and downconverted (bottom) CPL from UCNP-ChB hybrid composite films subjected to three cycles of heating and cooling.

nificance as these CTE active materials are in general hydrophilic and biocompatible, and hence can also be quoted as green luminescent materials with versatile applications.[26–28] Our material of interest, cholesteryl benzoate (ChB) (see chemical structure in Fig. 1), is a thermotropic cholesteric liquid crystalline (CLC) system which does not constitute any traditional luminescent moiety. While there have been efforts on controlling the phase changes in cholesteryl-based liquid crystalline derivatives in response to external stimuli, studies focusing on their ground and excited state optical activity is scarce.[29,30] Recently Zhou and coworkers explored CTE in ChB and investigated their excited state emissive properties in aggregated state.[31] Inspired from this work, we did systematic experimentations on understanding the phase changes in this class of materials as a function of external stimuli. Herein, we delve deeper into controlling the chiroptical properties in ChB by inducing phase changes under repeated heating–cooling cycles. Thermotropic chiral liquid crystalline properties coupled with clustering triggered emission is employed to demonstrate CPL activity in the visible region. Given that the template itself exhibit optical activity as well as luminescence, our objective is to generate both downconversion and upconversion CPL (UC-CPL) from a single material by employing ChB as the host chiral template and upconversion nanophosphors as the guest nanoparticle (Fig. 1). Lanthanide based upconversion nanophosphors (UCNPs), compared to conventional luminophores, have sharp emission peak, enhanced photostability as well as low toxicity, making it an ideal candidate for bioimaging assays and biomedical applications.[32] Recent advances in UC-CPL using liquid crystalline template have demonstrated multiple applications ranging from information storage, optical displays to security encryption.[33–35] Reported literatures have worked on tuning the photonic bandgap of achiral liquid crystalline material using chiral additives to form chiral template. In contrast, our approach is focused on (i) attaining CPL with enhanced g_{lum} using chiral cholesteric liquid crystal with multiple heating–cooling cycles and (ii) extending these efforts to generate multicolour UC-CPL by fabricating composite films using UCNPs.

Results and discussion

ChB, a thermotropic liquid crystal, is chosen as both source of chiral luminescence as well as a chiral host. The detailed investigation on the temperature-dependent photophysical and chiroptical properties of ChB was carried out using UV-visible spectroscopy, photoluminescence (PL) spectroscopy and CPL studies. The UV-visible spectrum of ChB in THF showed major absorption peaks at 242 and 273 nm corresponding to the benzoate side chain (Fig. 2a). The former peak is attributed to π–π* transition of benzene and the latter peak correlate to n–π* transition of ester functional group present in benzoate side chain. Inset in Fig. 2a shows the appearance of shoulder peak around 300 to 360 nm at higher concentration (0.1 M) of ChB, arising due to the aggregation of molecules. PL studies of ChB (0.1 M) revealed excitation-dependent emission properties in solution state (Fig. 2b). Given the material is a CTE luminogen forming higher order aggregates, prominent PL was observed at higher excitation wavelength (above 300 nm). A gradual red-shift was observed upon increasing the excitation wavelength due to the formation of different types of aggregates in solution (Fig. 2b & c). Maximum emission intensity was observed at 337 nm upon excitation at 300 nm.

The ChB clusters increase gradually with concentration, indicating progressive aggregation. These cluster chromophores are found to be of different sizes leading to differing electronic interactions and hence, exhibiting excitation-dependent emission.[36] Excitation spectra collected for ChB in THF showed intense peak at 300 nm under 337 nm emission, consistent with the absorption peaks (Fig. S1†). While the molecule possesses inherent chirality and showed CTE behaviour in solution state, it did not exhibit chiral emission, indicating lack of definite chiral arrangement within the structures (Fig. 2d).

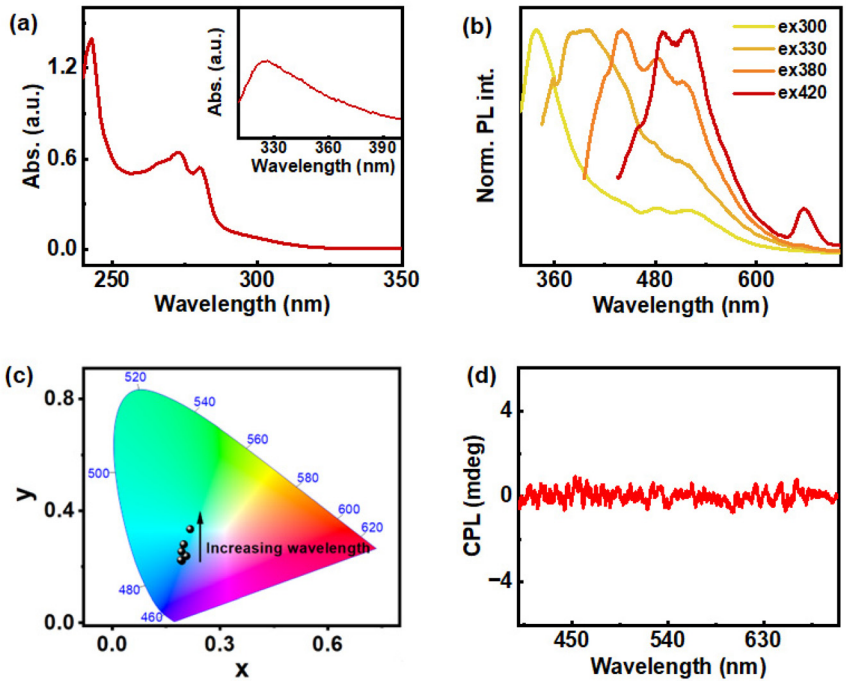

Fig. 2 Photophysical characterisation of ChB in THF; (a) UV-visible absorption, (b) excitation dependent emission, (c) chromaticity diagram of excitation dependent PL, and (d) CPL spectra at 300 nm excitation.

We further extended our studies to solid state wherein exciting changes in the chiroptical properties of ChB was identified under repeated heating cooling cycles. Physical properties of cholesteric liquid crystals are sensitive to temperature variation, and hence these materials are found to have diverse applications using temperature as stimulus.[38,42] PL of ChB in solid state coated on a glass slide upon three cycles of heating (to 186 °C) and cooling (to room temperature) at the rate of 2.5 °C per min, displayed excitation-dependent emission properties (Fig. S2†). Careful analysis of the data showed a gradual redshift in the emission peak with increase in excitation wavelength. The material showed a broad emission spanning from 400 to 600 nm and the emission maxima shifting from 420 to 500 nm. The spectra also displayed redshift with increasing number of heating cooling cycles for a particular excitation wavelength. This effect was particularly noticed at lower excitation wavelength (300 nm to 360 nm), and as excitation wavelength increases (>360 nm), only negligible change in PL maxima could be observed. In order to compare the emission efficiency in solution and solid state, absolute fluorescence quantum yield (QY) was measured in homogenous solution of ChB prepared in THF (0.2 M) with different excitation wavelength ranging from 300–420 nm. The sample exhibited a low QY in the range of 1–2%. In contrast, the solid state QY increased drastically to 8.62%, 6.94% and 6.46% for first, second and third cycles, respectively. An appreciable luminescence QY in the solid state opens avenue for the exploration of chiroptical properties in the excited state. The monomers are closer to each other in the solid state facilitating intramolecular interaction between the cluster chromophores thereby displaying intense PL, a phenomenon typical of the CTE effect. Furthermore, lifetime measurements carried out on the solid-state ChB after each thermal cycle at 416 nm excitation showed fits with a triexponential decay function (Fig. S3†). The average fluorescence lifetime was found to be 5.23 ns, 5.14 ns and 5.6 ns for first, second and third cycle respectively. Lack of appreciable changes in the lifetime upon repeated heating–cooling cycle indicates the robustness of the material throughout the process.

While emission due to CTE effect was observed in solid state ChB, the liquid crystalline property of the material can contribute to selective reflection. To further study these properties across each thermal cycle, absorption and diffused reflectance circular dichroism (DRCD) was measured. Solid state UV-visible absorption collected across repeated thermal cycles exhibited similar peaks for the three cycles of heating–cooling ranging from 200 nm to 420 nm (Fig. 3a). The absorption profile of first cycle is slightly different from second and third, wherein an increment in absorbance around 390–420 range was observed suggesting alternation in physical properties of cluster chromophores upon thermal treatment. Due to the selective reflectance property of liquid crystalline material, the circularly polarised light corresponding to photonic bandgap of the material with same handedness is reflected, while that of the opposite handedness is transmitted. DRCD provides information about the light reflected by the sample. The DRCD exhibited negative signal around 300–420 peak for second and third cycles with g_{abs} of 0.02 and 0.06 respectively, corroborating earlier observations of enhanced chiroptical properties on subjecting to multiple heating–cooling cycles (Fig. 3b).

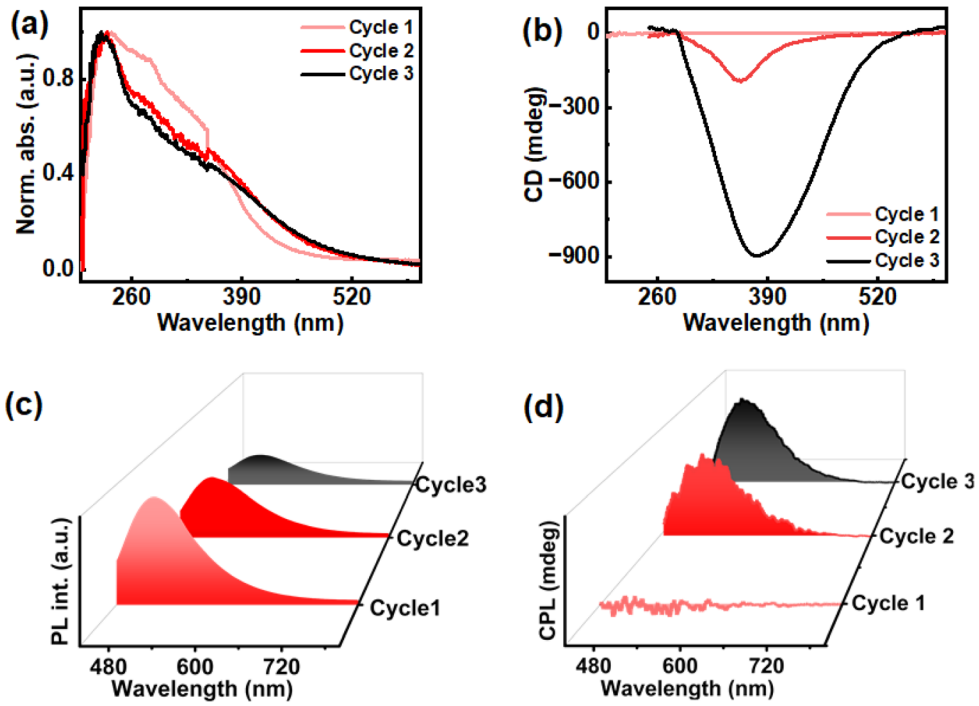

Fig. 3 (a) UV-visible absorption and (b) the corresponding DRCD spectra of ChB collected after multiple thermal cycles. (c) PL and (d) the corresponding CPL spectra of ChB collected after multiple thermal cycles (excitation wavelength = 416 nm).

The dual property of cholesteryl mesogens, chirality and luminescence, allows us to study the excited state chirality of ChB. The material demonstrated excitation-dependent CPL after the third cycle of slow heating and cooling (2.5 °C per min). The first cycle showed no noticeable CPL whereas signals emerged after the second cycle. Finally, a clear CPL signal was observed after the third cycle of heating–cooling. Since no significant increase in g_{lum} was observed beyond this cycle, thorough investigation was carried out until the third cycle. The highest g_{lum} value of 8.6×10^{-2} was observed after the third cycle under 416 nm excitation. The emission maxima of the film displayed no noticeable shift from 500 nm across all cycles when excited at 416 nm (Fig. 3c & d). Additionally, in order to rule out linear birefringence effect, CPL measurement was carried out on multiple points as well as by flipping the substrate (Fig. S4 & Table S1†). Consistency in signal intensity and g_{lum} values ruled out any contribution from the linear polarization effect to the observed CPL signals. To further explore the underlying causes of emission and chiral characteristics, temperature dependent experiments were carried out using consistent rates of heating and cooling. Thermogravimetric analysis performed to check the temperature stability of the material, both in real gas and nitrogen purged atmosphere, revealed no significant mass change with respect to temperature suggesting that the material remains intact during three cycles of heating and cooling (Fig. S5†).

In order to unravel the underlying mechanism of chiral emission, differential scanning calorimetry (DSC) was employed. DSC provided a deeper insight on liquid crystalline phase changes with respect to temperature across different cycles. DSC studies displayed two endothermic peaks while heating; the first corresponding to the transition from crystalline phase to cholesteric phase (N*) and the other corresponding to the cholesteric phase to isotropic liquid phase. Upon cooling, first exothermic peak refers to transition of isotropic liquid phase to N* whereas the second peak corresponds to transition of N* to crystalline phase. The DSC thermogram of the second and third cycles look similar, but noticeable changes where observed compared to the first. The phase transition temperature from crystalline to chiral nematic phase occurred at 151.70 °C in the first cycle of heating whereas the same was observed at 146.53 °C, 5.17 °C lower than the former, for second and third cycles (Fig. 4a). Decrement in transition temperature could be corroborated to thermal history of the sample where repeated heating–cooling at a slow rate can cause alterations in molecular orientation and packing.[45] The phase transition temperature of cholesteric phase to isotropic liquid phase was in the range of 180.35 °C for all thermal cycles (Fig. 4b). For cooling cycles, the first peak corresponding to transition of isotropic liquid to N* phase was at 179.95 °C (Fig. 4b) for each of the heating–cooling cycles.

On the other hand, the temperature corresponding to transition from N* to crystalline phase of the material was around 129.95 °C for all the thermal cycles. Polarized optical microscopy (POM) images of the films captured following each heating and cooling cycle (Fig. 4c, d and Fig. S6†) clarified the differences in texture of the material across thermal cycles. Notably, POM images of films prepared after the initial and

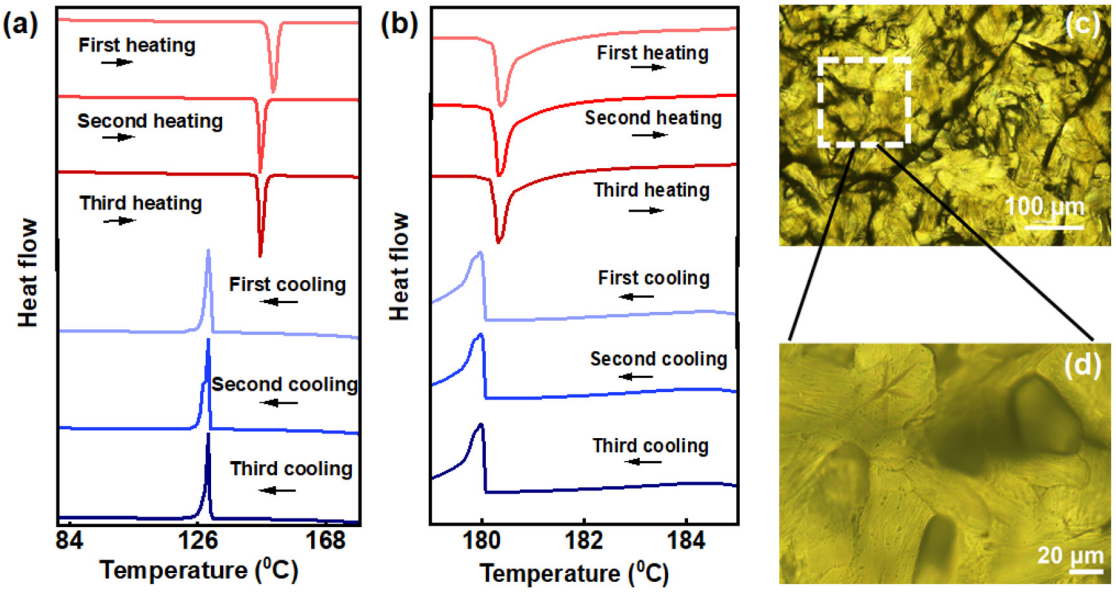

Fig. 4 DSC thermogram of ChB during each heating and cooling cycle. (a) Peak corresponding to transition from crystalline to liquid crystalline state (heating cycle; red traces) and *vice versa* (cooling cycle; blue traces). (b) Peak corresponding to transition from liquid crystalline state to isotropic liquid state (heating cycle; red traces) and *vice versa* (cooling cycle; blue traces). POM images of ChB after first cycle of heating cooling with magnification of (c) 5× and (d) 10×.

subsequent cycles reveal distinct patterns. After the first heating and cooling cycle, the liquid crystal film exhibited a fingerprint texture (Fig. 4c & d).[37] Subsequent cycles showed cold blue phase structure which represents a frustrated phase situated between the isotropic and chiral nematic state (Fig. S6†).[39] During the first cycle of heating and cooling, a disordered arrangement was observed, transitioning to an ordered chiral liquid crystalline arrangement with successive cycles. The emissive nature of ChB, combined with a well-ordered chiral arrangement following multiple heating and

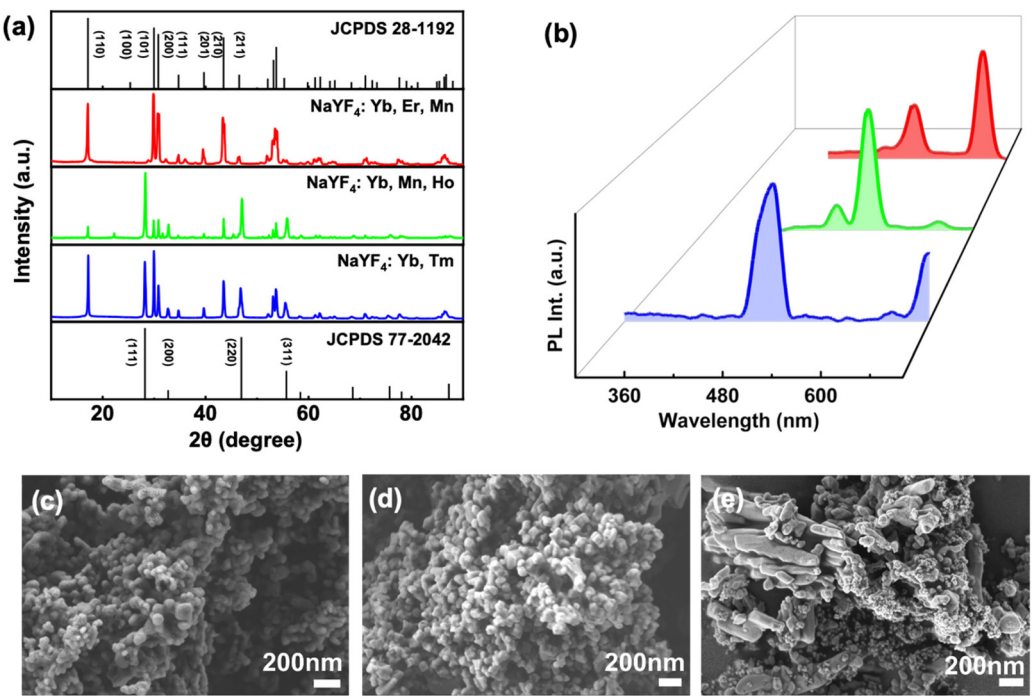

Fig. 5 (a) PXRD and (b) PL plots of $NaYF_4$/Yb,Tm (blue), $NaYF_4$/Yb,Mn,Ho (green), and $NaYF_4$/Yb,Er,Mn (red) UCNPs. SEM images of (c) blue, (d) green and (e) red emitting UCNPs.

cooling cycles, results in CPL property with a high anisotropy in luminescence.

Having established efficient down converted CPL in ChB, the next objective was to generate upconverted chiral emission from the same system. This could be achieved by using ChB as an effective template for incorporating luminescent guest materials. Considering their versatile applicability and thermal stability, lanthanide based UCNPs were chosen as desired luminophore.[40] Lanthanide based UCNPs capped by L-pyroglutamic acid (L-PGA) exhibiting blue (0.1 g L-PGA capped $NaYF_4$/Yb,Tm), green (0.5 g L-PGA capped $NaYF_4$/Yb, Mn,Ho) and red (0.1 g L-PGA capped $NaYF_4$/Yb,Er,Mn) emission was synthesised using a modified literature procedure.[41]

Structural characterisation of synthesised UCNPs was done using SEM imaging (Fig. 5c–e). The average size of UCNPs was estimated to be around 76 nm for $NaYF_4$/Yb,Tm, 77 nm for $NaYF_4$/Yb,Mn,Ho, and 92 nm for $NaYF_4$/Yb,Er. The $NaYF_4$/Yb, Tm UCNPs exhibited spherical morphology with uneven size ranges. However, in case of $NaYF_4$/Yb,Mn,Ho, increased ligand concentration resulted in spherical particles of uniform morphology. Red emitting $NaYF_4$/Yb,Er,Mn UCNPs formed irregular shaped particles with much bigger size. Further characterisation of UCNPs were carried out using powder X-ray diffraction (PXRD) measurements (Fig. 5a). Upon comparison with standard JCPDS files for $NaYF_4$ crystal lattice, cubic lattice patterns with peaks are at (111), (200), (220), (311) and hexagonal lattice diffraction peaks attributed at (110), (101), (200), (111), (201), (211) were observed in UCNPs. While $NaYF_4$/Yb,Tm showed both diffraction peaks equally, $NaYF_4$/Yb,Ho,Mn and $NaYF_4$/Yb,Er,Mn UCNPs showed predominantly cubic and hexagonal morphology, respectively. As expected, none of the diffraction patterns showed peaks corresponding to Yb, Er, Mn, and Ho due to its low concentration compared to that of Na, Y, and F. The surface charge for each of these nanophosphors was identified using zeta potential measurements. All nanophosphors exhibited positive surface charge with 33.8 mV, 25 mV and 21.1 mV for the blue, green and red emitting UCNPs, respectively (Fig. S7†).

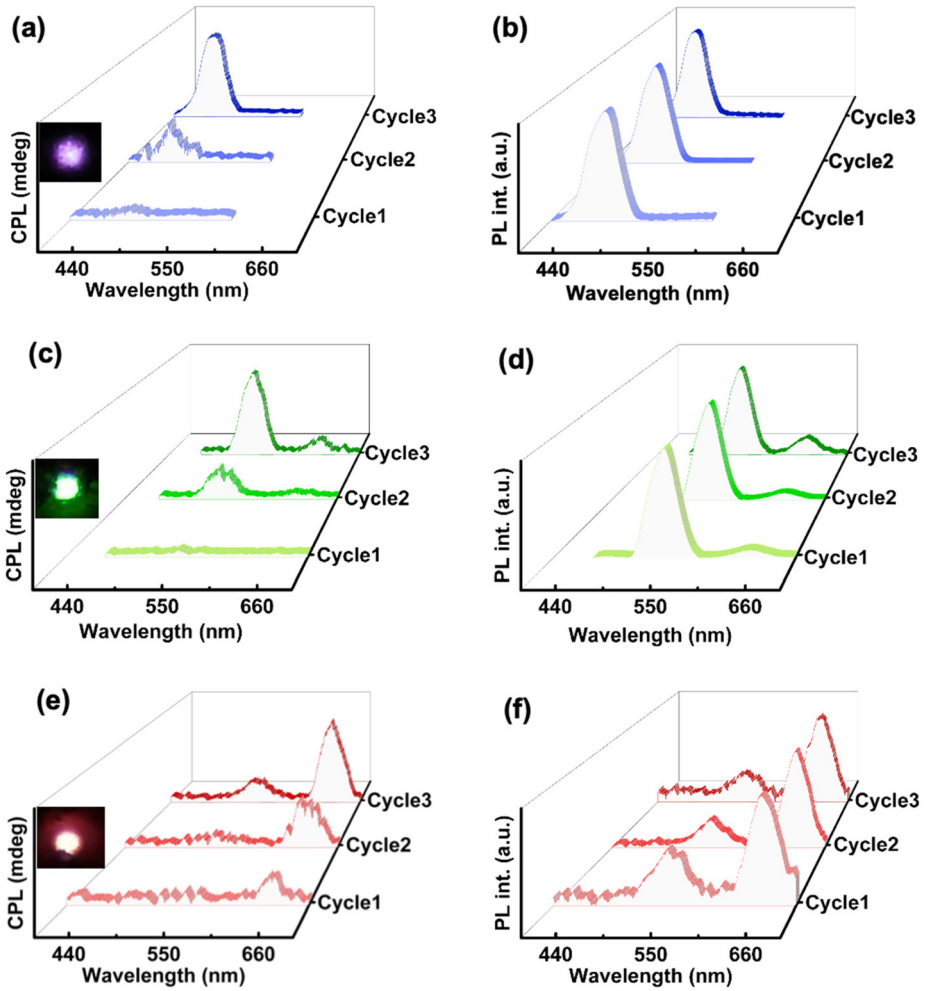

Fig. 6 (a, c and e) CPL and (b, d and f) PL spectra of UCNP-ChB nanocomposites collected from films prepared by incorporating $NaYF_4$/Yb,Tm (blue traces), $NaYF_4$/Yb,Mn,Ho (green traces) and $NaYF_4$/Yb,Er,Mn (red traces) into the ChB. The spectra were collected for different thermal cycles after excitation using a 980 nm diode laser. Inset shows the photograph of film irradiated with the laser.

The photophysical characterisation of UCNPs was carried using UV-visible and PL spectroscopy. Solid-state absorption of UCNPs showed a sharp in the NIR region around 980 nm (Fig. S8†). To analyse the PL in solution state, dried samples at a concentration of 1 mg mL^{-1} were dissolved in ethanol. L-PGA capped blue emitting UCNPs showed a major peak around 480 nm and a minor peak around 700 nm upon excitation using a 980 nm laser (Fig. 5b). The peak at 480 nm corresponds to transition from $^1G_4$ to $^3H_6$ whereas the one at 700 nm arises from the $^3F_{2/3}$ to $^3H_6$ transition in Tm^{3+}. In case of L-PGA capped green emitting UCNPs in which Ho^{3+} is the activator, a peak at 530 nm corresponding to $^5S_2$ to $^1I_8$ transition and another peak at 640 nm corresponding to $^5F_5$ to $^1I_8$ were observed. For L-PGA capped red emitting $NaYF_4$/Yb,Er,Mn UCNPs, the transitions from the $^2H_{11/2}$, $^4S_{3/2}$, and $^4F_{9/2}$ excited levels to the $^4I_{15/2}$ ground state of Er^{3+} are responsible for the green (528 nm, 545 nm) and red (660 nm) emission, respectively.

For the fabrication of hybrid nanocomposites, UCNPs were incorporated into ChB followed by grinding, mixing, and subsequently heating–cooling on glass substrate. Similar to the ChB substrate, nanocomposites containing different UCNPs were subjected to three cycles of slow heating and cooling. The POM images of the nanocomposites showed that the liquid crystalline nature of the template remained intact even after the incorporation of the nanophosphors (Fig. S9†). Similar to ChB texture (*vide supra*), the UCNP incorporated samples exhibited a fingerprint nature after first thermal cycle which was followed by uniform mesogenic arrangement in the consecutive cycles. The samples were further analysed for their chiral emissive performance upon exciting using a 980 nm NIR laser. The spectra remained CPL silent after the first cycle of heating–cooling. Interestingly, emergence of CPL signal could be observed in the second cycle with a g_{lum} in the range of 10^{-2}. The CPL intensity and the anisotropy value enhanced by an order of magnitude after the third cycle with observed g_{lum} of 0.36, 0.24 and 0.11 for blue, green and red emitting UCNPs, respectively (Fig. 6). The optimised weight percentages of UCNPs (composite films with maximum g_{lum}) used with respect to ChB in case blue, green and red emitting UCNPs respectively were 20 wt%, 40 wt% and 20 wt%, respectively. Measurements were taken by flipping the sample and from different points in order to rule out any contribution from linear birefringence effect (Fig. S10 & S11†). UC-CPL signals covering the blue, green and red regions of electromagnetic spectrum could be achieved by using different nanophosphors. The high luminescence anisotropy values combined with tunability of wavelength highlights the potential of such substrates in generating intense chiral emission for practical application in display devices. Control experiments with pure ChB films showed no PL or CPL across all cycles of heating–cooling under 980 nm excitation indicating that the CPL signals observed with NIR excitation are exclusively from UCNPs (Fig. S12†).

The unique combination of chirality and luminescence from the ChB template offers diverse platforms. In addition to

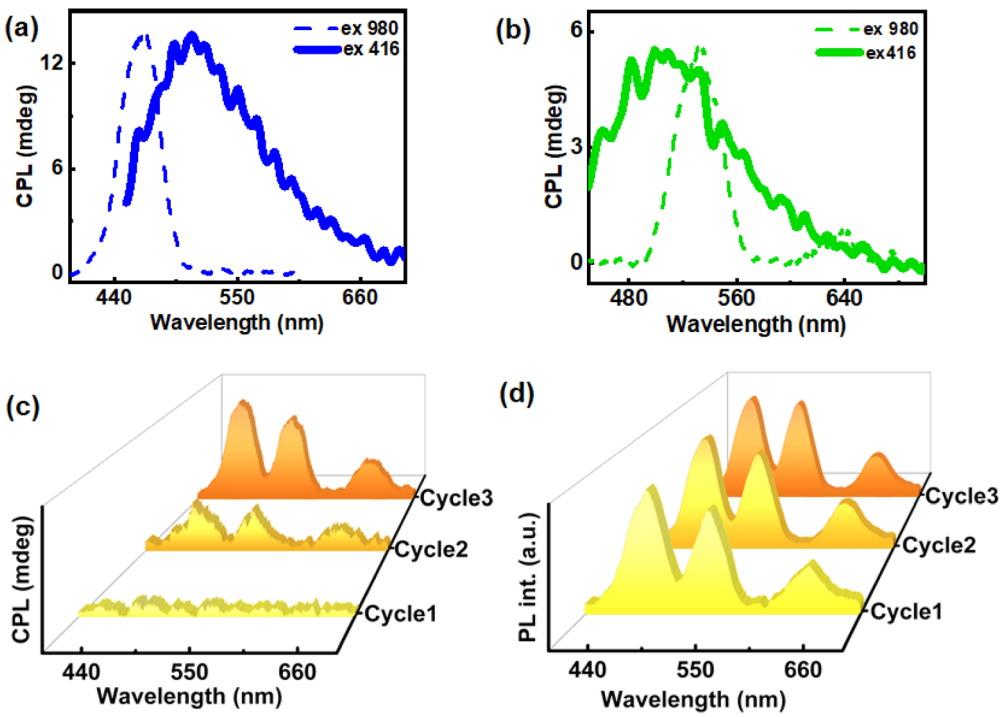

Fig. 7 Downconversion CPL (solid lines) and upconversion CPL (dashed lines) from composite films formed from ChB and UCNPs; (a) ChB-NaYF4/Yb,Tm and (b) ChB-NaYF4/Yb,Mn,Ho films. (c) Multicolour CPL and (d) PL of ChB-UCNP film composed of all the threes UCNPs (excitation wavelength = 980 nm).

the intense UC-CPL signals observed, the intrinsic nature of the fabricated films offers the possibility of conventional downconversion CPL. Since the template also exhibits chiral emission after multiple thermal cycles, CPL performance of UCNP-ChB film under 416 nm excitation was recorded. The film displayed CPL around 450 to 560 nm with g_{lum} values of 5.5×10^{-2}, 8×10^{-2}, 7.9×10^{-3} for blue, green and red emitting UCNPs incorporated ChB films, respectively (Fig. 7a, b & S13†). Hence, we demonstrate the successful switching of the upconversion CPL (λ_{ex} = 980 nm; dashed lines in Fig. 7a and b) and downconversion CPL (λ_{ex} = 416 nm; solid lines in Fig. 7a and b) from the same composite film by mere alteration of excitation wavelength. ChB demonstrates versatility in accommodating UCNPs of various shapes and sizes, rendering it a promising candidate for generating broad-spectrum UC-CPL across the entire visible region. CPL spectra covering the entire visible region, owing to its applications in smart windows and anticounterfeiting techniques, is gaining vast interest in recent years.[43,44] Achieving broad emission poses a challenge within the UCNP system due to its sharp emission peaks. To showcase multicolour CPL from UCNP-ChB film, UCNPs exhibiting blue, green and red emission were dissolved in ethanol at a ratio of 1.5 : 1 : 1.7 and allowed to evaporate undisturbed in an oven (at 120 °C). Once dried, the UCNP mixture was grinded and mixed well with ChB at 30 wt% and performed three thermal cycles (see ESI†). Excitation using a 980 nm laser prompted emission from all three UCNPs. Interestingly, a gradual increase in the CPL intensity could be achieved upon subsequent heating–cooling cycles. Clear CPL signals covering the three primary colours could be observed after third thermal cycle with an average g_{lum} of 0.14 (Fig. 7c & d). To the best of our knowledge, this is the first successful demonstration of broadband multicolour UC-CPL from chiral luminescent nanocomposites. This system having multicolour UC-CPL with high g_{lum} can be made more efficient and general by fabricating polymer stabilised films.

Conclusion

In conclusion, we have developed a facile approach to fabricate nanomaterials exhibiting downconverting and upconverting CPL within the same liquid crystalline template. This strategy allows demonstrating CPL in a green luminescent CTE based luminogen, namely ChB, without tedious synthetic protocols, opening avenues for easy design of chiral emissive non-conventional thermotropic liquid crystalline materials. The downconversion CPL was observed in ChB upon repeated heating–cooling cycles, attributed to its CTE and chiral organization in response to thermal variations. The CPL signals from ChB exhibited excitation dependence with g_{lum} reaching as high as 0.086. Furthermore, UC-CPL with multiple chiral emission colours could be achieved by fabricating ChB-UCNP hybrid nanocomposites. Successful incorporation of multicolour emissive UCNPs paves the way for UC-CPL covering the whole visible region with a dissymmetry factor as high as 0.36. Low toxicity, biocompatible nature of both template and nanomaterial along with intense and tunable chiral luminescence makes the system ideal for bionanomaterial applications. Upgrading the system by manufacturing polymer stabilised self-standing films can have potential applications in numerous fields including optical displays.

Data availability

The data supporting this article have been included as part of the ESI.†

Author contributions

J. K. conceived and coordinated the project. S. T. N., A. M. and S. M. carried out the experiments. S. T. N. and J. K. analysed the data. S. T. N. and J. K. prepared the manuscript. All authors have given approval to the final version of the manuscript.

Conflicts of interest

The authors declare no competing financial interest.

Acknowledgements

J. K. acknowledges financial support from Council of Scientific and Industrial Research (CSIR), India [Project No. 01(3029)/21/EMR-II]. S. T. N. and S. M. acknowledge DST-INSPIRE, and A. M. acknowledges DST Nanomission (Grant DST/NM/TUE/EE-03/2019-1G-IISERTp) for fellowship. The authors thank the Department of Chemistry, IIT Tirupati for reflectance measurements, and Dr Ravi Kumar Pujala, Mr Surya Narayana Sangitra, and Mr G. Nazeer Ahmed, Department of Physics, IISER Tirupati, for their help with POM imaging. Our sincere gratitude to Dr Santhosh Babu Sukumaran and Ashwini Narayanan, Department of Chemical Science, NCL Pune, for DSC measurements. The authors acknowledge IISER Tirupati for providing research facilities.

References

1 P. Stachelek, L. Mackenzie, D. Parker and R. Pal, *Nat. Commun.*, 2022, **13**, 5532022.
2 Q. Guo, M. Zhang, Z. Tong, S. Zhao, Y. Zhou, Y. Wang, S. Jin, J. Zhang, H. B. Yao, M. Zhu and T. Zhuang, *J. Am. Chem. Soc.*, 2023, **145**, 4246–4253.
3 K. Dhbaibi, L. Abella, S. Meunier-Della-Gatta, T. Roisnel, N. Vanthuyne, B. Jamoussi, G. Pieters, B. Racine, E. Quesnel, J. Autschbach and J. Crassous, *Chem. Sci.*, 2021, **12**, 5522–5533.

4 Y. Kitagawa, S. Wada, M. J. Islam, K. Saita, M. Gon, K. Fushimi, K. Tanaka, S. Maeda and Y. Hasegawa, *Commun. Chem.*, 2020, **3**, 119.
5 C. Hao, L. Xu, M. Sun, H. Zhang, H. Kuang and C. Xu, *Chem. – Eur. J.*, 2019, **25**, 12235–12240.
6 Y. Zhang, S. Yu, B. Han, Y. Zhou, X. Zhang, X. Gao and Z. Tang, *Matter*, 2022, **5**, 837–875.
7 Y. Imai, Y. Nakano, T. Kawai and J. Yuasa, *Angew. Chem., Int. Ed.*, 2018, **57**, 8973–8978.
8 C. Han and H. Li, *Small*, 2008, **4**, 1344–1350.
9 I. Sato, R. Sugie, Y. Matsueda, Y. Furumura and K. Soai, *Angew. Chem., Int. Ed.*, 2004, **43**, 4490–4492.
10 Y. Yang, R. C. Da Costa, M. J. Fuchter and A. J. Campbell, *Nat. Photonics*, 2013, **7**, 634–638.
11 D. Y. Kim, *J. Korean Phys. Soc.*, 2006, **49**, 505.
12 S. Maniappan, C. Dutta, D. M. Solís, J. M. Taboada and J. Kumar, *Angew. Chem., Int. Ed.*, 2023, **62**, e202300461.
13 G. González-Rubio, J. Mosquera, V. Kumar, A. Pedrazo-Tardajos, P. Llombart, D. M. Solís, I. Lobato, E. G. Noya, A. Guerrero-Martínez, J. M. Taboada and F. Obelleiro, *Science*, 2020, **368**, 1472–1477.
14 S. Maniappan, K. L. Reddy and J. Kumar, *Chem. Sci.*, 2023, **14**, 491–498.
15 C. Dutta, S. Maniappan and J. Kumar, *Chem. Sci.*, 2023, **14**, 5593–5601.
16 Y. Sang, J. Han, T. Zhao, P. Duan and M. Liu, *Adv. Mater.*, 2020, **32**, 1900110.
17 Y. Wu, M. Li, Z. G. Zheng, Z. Q. Yu and W. H. Zhu, *J. Am. Chem. Soc.*, 2023, **145**, 12951–12966.
18 M. Nakamura, F. Ota, T. Takada, K. Akagi and K. Yamana, *Chirality*, 2018, **30**, 602–608.
19 J. Sharma, R. Chhabra, A. Cheng, J. Brownell, Y. Liu and H. Yan, *Science*, 2009, **323**, 112–116.
20 X. Wu, L. Xu, L. Liu, W. Ma, H. Yin, H. Kuang, L. Wang, C. Xu and N. A. Kotov, *J. Am. Chem. Soc.*, 2013, **135**, 18629–18636.
21 A. D. Merg, J. C. Boatz, A. Mandal, G. Zhao, S. Mokashi-Punekar, C. Liu, X. Wang, P. Zhang, P. C. van der Wel and N. L. Rosi, *J. Am. Chem. Soc.*, 2016, **138**, 13655–13663.
22 A. Terech and R. G. Weiss, *Chem. Rev.*, 1997, **97**, 3133–3160.
23 K. L. Reddy, J. P. Mathew, S. Maniappan, C. Tom, E. Shiby, R. K. Pujala and J. Kumar, *Nanoscale*, 2022, **14**, 4946–4956.
24 Y. Zhao, J. Long, P. Zhuang, Y. Ji, C. He and H. Wang, *J. Mater. Chem. C*, 2022, **10**, 1010–1016.
25 F. Kausar, Z. Zhao, T. Yang, W. Hou, Y. Li, Y. Zhang and W. Z. Yuan, *Macromol. Rapid Commun.*, 2021, **42**, 2100036.
26 X. Zhan, F. F. Xu, Z. Zhou, Y. Yan, J. Yao and Y. S. Zhao, *Adv. Mater.*, 2021, **33**, 2104418.
27 D. Wang and B. Z. Tang, *Acc. Chem. Res.*, 2019, **52**, 2559–2570.
28 Z. Zhang, M. Kang, H. Tan, N. Song, M. Li, P. Xiao, D. Yan, L. Zhang, D. Wang and B. Z. Tang, *Chem. Soc. Rev.*, 2022, **51**, 1983–2030.
29 T. Itahara, S. Furukawa, K. Kubota, M. Morimoto and M. Sunose, *Liq. Cryst.*, 2013, **40**, 589–598.
30 J. Li, Y. Cong, H. Huang, Q. Shi, Y. Jia and B. Zhang, *New J. Chem.*, 2022, **46**, 9024–9035.
31 M. Zhou, Y. Gong, Y. Yuan and H. Zhang, *J. Phys. Chem. C*, 2022, **126**, 15485–15490.
32 K. L. Reddy, R. Balaji, A. Kumar and V. Krishnan, *Small*, 2018, **14**, 1801304.
33 X. Yang, M. Zhou, Y. Wang and P. Duan, *Adv. Mater.*, 2020, **32**, 2000820.
34 X. Yang, X. Jin, A. Zheng and P. Duan, *ACS Nano*, 2023, **17**, 2661–2668.
35 C. Jiang, Y. Shi, X. Yang, T. Zhao, J. Zhou, X. Jin, Y. Zhang and P. Duan, *Adv. Opt. Mater.*, 2023, 2300001.
36 Z. Zhao, X. Chen, Q. Wang, T. Yang, Y. Zhang and W. Z. Yuan, *Polym. Chem.*, 2019, **10**, 3639–3646.
37 Y. Wu, L. H. You, Z. Q. Yu, J. H. Wang, Z. Meng, Y. Liu, X. S. Li, K. Fu, X. K. Ren and B. Z. Tang, *ACS Mater. Lett.*, 2020, **2**, 505–5102020.
38 W. Zhang, A. A. Froyen, A. P. Schenning, G. Zhou, M. G. Debije and L. T. de Haan, *Adv. Photonics Res.*, 2021, **2**, 2100016.
39 I. Dierking, *Textures of Liquid Crystals*, Wiley-VCH, Weinheim, 2003.
40 G. Chen, H. Qiu, P. N. Prasad and X. Chen, *Chem. Rev.*, 2014, **114**, 5161–5214.
41 K. L. Reddy, J. P. Mathew, E. Shiby and J. Kumar, *J. Phys. Chem. C*, 2021, **125**, 26263–26273.
42 A. Bobrovsky, A. Piryazev, D. Ivanov, M. Kozlov and V. Utochnikova, *Polymers*, 2023, **15**, 1344.
43 Y. Shi, J. Han, C. Li, T. Zhao, X. Jin and P. Duan, *Nat. Commun.*, 2023, **14**, 6123.
44 C. Jiang, Y. Shi, X. Yang, T. Zhao, J. Zhou, X. Jin, Y. Zhang and P. Duan, *Adv. Opt. Mater.*, 2023, 2300001.
45 T. Tip, *Interpreting DSC Curves Part 1: Dynamic Measurements.*, Accessed 01 August 2023, Available online: **https://www.eng.uc.edu/~beaucag/Classes/Character**.